Delayed thermalization in the mass-deformed Sachdev-Ye-Kitaev model

Dillip Kumar Nandy,[1,*] Tilen Čadež,[1,†] Barbara Dietz,[1,‡] Alexei Andreanov,[1,2,§] and Dario Rosa[1,2,‖]
[1]*Center for Theoretical Physics of Complex Systems, Institute for Basic Science (IBS), Daejeon 34126, Korea*
[2]*Basic Science Program, Korea University of Science and Technology (UST), Daejeon 34113, Korea*

(Received 28 June 2022; revised 19 December 2022; accepted 20 December 2022; published 28 December 2022)

We study the thermalizing properties of the mass-deformed Sachdev-Ye-Kitaev model, in a regime of parameters where the eigenstates are ergodically extended over just portions of the full Fock space, as an all-to-all toy model of many-body localization (MBL). Our numerical results strongly support the hypothesis that, although considerably delayed, thermalization is still present in this regime. Our results add to recent studies indicating that MBL should be interpreted as a strict Fock-space localization.

DOI: 10.1103/PhysRevB.106.245147

I. INTRODUCTION

The prospect of finding isolated quantum many-body systems capable of escaping from thermalization, currently understood in the framework of the eigenstate thermalization hypothesis (ETH) [1–3], has been one of the central aspects of research in condensed matter physics over the last two decades. In typical thermalizing systems, any memory of an initial configuration quickly evolves into highly nonlocal degrees of freedom and is lost to a large extent. Identifying systems defying thermalization has become even more pressing in the last few years, with the recent advances in building quantum computers and other nanodevices. Such systems, able to preserve information about their initial configurations, are of uttermost importance to implement concrete realizations of quantum memory.

An obvious way to evade thermalization is to consider integrable systems. However, they are generically very sensitive to perturbations, and even small imperfections—unavoidable in practical realizations—are enough to spoil integrability and restore thermalization. It has been understood since the seminal work of Anderson [4] that disorder can provide a robust mechanism to avoid thermalization. Anderson localization has been studied extensively in subsequent years, leading to many numerical and exact results which are by now well established and accepted [5,6]. For example, it has been proven mathematically that, in any dimension and for large enough disorder, localization occurs [7], and in $d = 1$, any infinitesimal uncorrelated disorder is enough to induce localization [8]. The same behavior is believed to hold in $d = 2$ as well [9], while in $d = 3$, the presence of a finite critical disorder has been largely established [5,6]. However, the Anderson problem is a single-particle problem and, as such, does not describe a realistic situation with many particles and interactions that cannot be neglected. Hence, it is natural to ask about the fate of Anderson localization in the presence of interactions.

To begin with, one has to define localization in a genuine many-body setup since the single-particle wave functions lose their significance, and one cannot simply state that a certain wave function is localized in space [10]. This problem has initially been addressed through the notion of *Fock-space localization* [11–13]. It is based on the observation that a generic disordered interacting many-body problem can be recast as an Anderson-like problem on a highly connected graph defined in Fock space. Hence, the study of the possibility of having eigenstates localized in Fock space makes sense. Systems enjoying Fock-space localization, usually referred to as many-body localization (MBL), display peculiar features, making them very different from systems obeying ETH. Examples are the absence of transport [14], area-law entangled eigenstates [15,16], a logarithmic growth of entanglement entropy after a quantum quench [10,17], Poissonian spectral correlations [18,19], and the emergence of an extensive set of local integrals of motion [15,20,21]. It was later argued that strict Fock-space localization was not necessary to display the phenomenological features of MBL listed above [16] and that, even in the presence of extended eigenstates in Fock space but with an extension much smaller than the dimension of the Hilbert space, the area-law entanglement entropy may emerge. This point of view was later confirmed numerically by the authors of Ref. [22], who investigated the paradigmatic example of the disordered Heisenberg model in one dimension (1D) [18,19]. According to their results, eigenstates in the MBL phase have nontrivial fractal dimension in Fock space, and they are not localized [23].

However, the absence of simple solvable models makes the understanding of MBL extremely challenging. Many results are either derived relying on some approximations or obtained numerically for relatively small system sizes, accessible to classical computers, which might not be enough to reach the thermodynamic limit [24–30].

A notable exception is represented by the so-called *mass-deformed Sachdev-Ye-Kitaev (SYK) model* [31,32], which is

*nandy@ibs.re.kr
†tilencadez@ibs.re.kr
‡barbara@ibs.re.kr
§aalexei@ibs.re.kr
‖dario_rosa@ibs.re.kr

a fully connected disordered interacting model modified to include a random mass term. This model, depending on the strength of the mass deformation, shows a transition from ergodic to localized in Fock space which can be studied analytically in the large-N limit [33,34]. In addition, for intermediate values of the mass deformation, eigenstates are restricted to (ergodically) cover energy shells in Fock space, whose dimensions are much smaller than the full Hilbert space dimension but still are exponentially large in N. By ergodically, we mean that, on a given energy shell, the eigenstate is homogeneously distributed. We will refer to this regime as the *cluster regime*. Hence, this model represents an excellent toy model of MBL, including the clustering property emphasized in Refs. [16,22], despite the model not having any spatial extension.

In this paper, we reanalyze numerically the mass-deformed SYK model, with a particular focus on understanding to which extent its ergodic properties are absent or present in the cluster regime. The numerical analysis is performed by means of the adiabatic gauge potential (AGP), introduced in Ref. [35] as a very sensitive probe of quantum chaos, which measures the response of eigenvectors under small deformations of the model. In agreement with Ref. [29], we show that the cluster regime can be characterized as a region where the scaling of AGP with system size is faster than the scaling predicted by ETH. In addition, we investigate the ergodic properties of this regime by studying the spectral form factor (SFF) and the associated notion of Thouless time. Our findings show that Thouless time has a scaling with system size which, for large enough systems, is comparable with that in the ergodic regime. Thus, our results suggest that, at least for this particular model, the cluster regime must be considered a delayed but still thermalizing regime. To observe a genuine violation of thermalization, one must consider the regime of Fock-space localization. Interestingly, very similar conclusions were reached in Ref. [36] for other systems (see also Refs. [37,38]).

The paper is organized as follows. In Sec. II, we recall the main features of the mass-deformed SYK model found in Refs. [33,34]. In Sec. III, we present our numerical results based on the evaluation of AGP. In Sec. IV, we use the SFF to show that the intermediate regime, in which eigenstates are extended over clusters of dimension scaling with N, is thermalizing. In Sec. V, we conclude our findings. In the Appendixes, we present a detailed comparison of our notations and definitions with the corresponding ones of Ref. [33], the AGP for a local deformation for comparison with the extensive one used in the main text, a more detailed analysis of the random matrix theory properties of the model under investigation (Appendix C) as well as a more detailed discussion of the SFF definition (Appendix D).

II. THE MODEL

The model under consideration has been dubbed in the literature as mass-deformed SYK [31–33,39,40]. As the name suggests, it can be thought of as a deformation of the celebrated SYK model [41–43], by adding a quadratic random mass term. It is realized in terms of N (with N being an even integer) Majorana fermions, $\hat{\chi}_i,\ i = 1, \ldots, N$, i.e., quantum mechanical operators satisfying Clifford algebra relations $\{\hat{\chi}_i,\ \hat{\chi}_j\} = \delta_{ij}$. The Hamiltonian reads

$$\begin{aligned}\hat{\mathcal{H}} &\equiv \frac{2}{\sqrt{N}}\hat{\mathcal{H}}_4 + \kappa\,\hat{\mathcal{H}}_2,\\ \hat{\mathcal{H}}_4 &= -\sum_{i<j<k<l} J_{ijkl}\hat{\chi}_i\hat{\chi}_j\hat{\chi}_k\hat{\chi}_l,\\ \hat{\mathcal{H}}_2 &= i\sum_{i<j} J_{ij}\hat{\chi}_i\hat{\chi}_j,\end{aligned} \tag{1}$$

where the coupling constants J_{ijkl} and J_{ij} are Gaussian distributed with vanishing mean values and variances given by $\frac{6}{N^3}$ and $\frac{1}{N}$, respectively. Finally, κ is the mass-deformation strength parameter, which controls the strength of the quadratic mass deformation compared with the quartic interaction term [44].

The model above has been studied in Refs. [33,34] as an analytically tractable model of Fock-space localization. As such, we are going to use it as a platform to benchmark various probes of the ETH/MBL transition used in the literature at finite values of N vs their large-N predictions in the thermodynamic limit. More in detail, Ref. [33] identified four major regimes as a function of κ (see also Ref. [45]):

(1) Regime I: $\kappa < \sqrt{\frac{(N-2)(N-3)}{2N^3}}$. Eigenstates are ergodically extended over the full Fock space, and ETH holds for all eigenstates.

(2) Regimes II and III—cluster regime: $\sqrt{\frac{(N-2)(N-3)}{2N^3}} < \kappa < \frac{Z}{2\sqrt{2\rho}}W(2Z\sqrt{\pi})$. Eigenstates are ergodically extended over energy shells whose dimension scales exponentially in N. This is the most interesting regime: a given eigenstate in the Fock space is extended to cover just the nearest neighbors (or a fraction of the nearest neighbors). Such a configuration, in standard Anderson problems in finite dimensions, would give rise to localization. However, since the connectivity of the mass-deformed model in the Fock space scales with N, these states still have an extensive support in Fock space.

The two regimes differ by the extension of the corresponding energy shells (which are exponentially extended in N in both cases): in regime II, all the nearest neighbors of a given unperturbed state are hybridized, while in regime III, only a fraction of the nearest neighbors are hybridized by the quartic terms. As discussed at length in Ref. [34], states in these regimes are homogeneously spread over the full accessible shell [46], implying absence of the so-called nonergodic extended states. The boundary between the two regions is located at $\kappa = \sqrt{\frac{6}{N^4}\binom{N}{4}}$.

(3) Regime IV—Fock-space localization: $\kappa > \frac{Z}{2\sqrt{2\rho}}W(2Z\sqrt{\pi})$. Eigenstates are localized in Fock space.

We define $Z \equiv \binom{N/2}{4}$ and $\rho \equiv \binom{N}{4}$, and W is the Lambert W function.

III. NUMERICAL RESULTS: AGP

The AGP has been proposed as a very sensitive probe of quantum chaos [35] (see also Refs. [47,48]). It measures the sensitivity of eigenstates to small perturbations of the Hamiltonian. In chaotic models, eigenstates are expected to

be very sensitive to deformations, distinct from integrable systems where such a sensitivity is supposed to be much smaller [49]. More quantitatively, let us consider a given Hamiltonian $\hat{\mathcal{H}}$ with eigenvectors $|n\rangle$ and energies E_n. We add a small deformation to $\hat{\mathcal{H}}$, $\hat{\mathcal{H}} \to \hat{\mathcal{H}}(\lambda) = \hat{\mathcal{H}} + \lambda\hat{O}$, where $\hat{O}$ is a generic operator which does not commute with $\hat{\mathcal{H}}$, and λ is a parameter. Then the AGP, denoted by $\|\mathcal{A}_\lambda\|^2$, is defined as follows (we keep the dependence on λ in $|n\rangle$ and E_n implicit):

$$\begin{aligned}\|\mathcal{A}_\lambda\|^2 &\equiv \frac{1}{D}\sum_{m\neq n} |\langle n|\hat{\mathcal{A}}_\lambda|m\rangle|^2,\\ \langle n|\hat{\mathcal{A}}_\lambda|m\rangle &\equiv -i\frac{\omega_{nm}}{\omega_{mn}^2+\mu^2}\,\langle n|\partial_\lambda\hat{\mathcal{H}}(\lambda)|m\rangle\\ &= -i\frac{\omega_{nm}}{\omega_{mn}^2+\mu^2}\,\langle n|\hat{O}|m\rangle,\end{aligned} \tag{2}$$

where ω_{mn} denotes the energy difference, $\omega_{mn} \equiv E_m - E_n$, μ is a regularizing cutoff at $E_m \sim E_n$, and D is the Hilbert space dimension.

The authors of Ref. [35] extensively studied the scaling properties of $\|\mathcal{A}_\lambda\|^2$ for several examples of integrable and chaotic systems. Their findings indicate that, in agreement with ETH, $\|\mathcal{A}_\lambda\|^2$ scales exponentially with the system size N when the system is thermalizing. On the other hand, the scaling with the system size is much milder for integrable systems, including the extreme case of free particles for which $\|\mathcal{A}_\lambda\|^2$ does not scale at all with the system size.

In the case at hand, we studied the behavior of $\|\mathcal{A}_\lambda(\kappa)\|^2$, as a function of κ, for the following extensive operator:

$$\hat{O} \equiv i\sum_{i=1}^{N-1} \hat{\chi}_i\hat{\chi}_{i+1}. \tag{3}$$

The choice for this operator is dictated by its simplicity: since the Hamiltonian, Eq. (1), preserves parity symmetry, any sensitive operator used to evaluate the AGP must be formed by products of even numbers of Majorana fermions. In addition, since the model is all-to-all and has no notion of locality, the results do not depend on which pairs of Majorana are considered.

Finally, we have checked that results are qualitatively unchanged when considering local (i.e., not extensive) operators (see Appendix B for an example).

For $\kappa = 0$, we recover the usual SYK model for which ETH holds [50,51]. Hence, to better investigate deviations from ETH behavior, we define the following modification of the AGP:

$$\|\tilde{\mathcal{A}}_\lambda(\kappa)\|^2 \equiv \frac{\|\mathcal{A}_\lambda(\kappa)\|^2}{\|\mathcal{A}_\lambda(0)\|^2}, \tag{4}$$

which we refer to simply as AGP in the following. From its definition, $\|\tilde{\mathcal{A}}_\lambda(\kappa)\|^2$ is expected to be N independent in the ETH region, i.e., for small values of κ. On the other hand, for very large values of κ, where Fock-space localization sets in, $\|\mathcal{A}_\lambda(\kappa)\|^2$ is expected to be largely independent of N, so that $\|\tilde{\mathcal{A}}_\lambda(\kappa)\|^2$ is expected to scale down exponentially with system size.

Based on these premises, we have computed $\|\tilde{\mathcal{A}}_\lambda(\kappa)\|^2$ for system sizes ranging from $N = 22$ to 30. Results of our numerical analysis are summarized in Fig. 1. We see that both

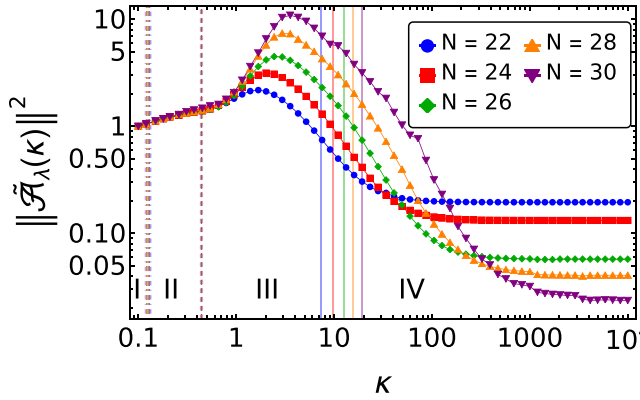

FIG. 1. The behavior of the adiabatic gauge potential (AGP), as a function of the mass deformation strength κ. Results are obtained by considering infinite temperature eigenstates, i.e., eigenstates having energies $-0.05 < E < 0.05$. Vertical lines show regime boundaries (colors reflect the N dependence of such boundaries): solid lines refer to boundaries between regimes III and IV, dashed lines to boundaries between regimes II and III, and dot-dashed lines to boundaries between regimes I and II.

regimes I and II follow quite closely the prediction of ETH, with the curves collapsing on top of each other. Similarly, for large values of disorder, the AGP is κ independent and inversely proportional to N, as expected for a free theory. Interestingly, we observe that the value of κ at which Fock-space localization becomes manifest is systematically larger than the large-N value predicted in Ref. [33].

In Ref. [35], the authors extensively addressed this point by considering the case of an integrable many-body Hamiltonian perturbed by a small nonintegrable perturbation. They found that AGP detects the chaotic transition for a strength of the nonintegrable deformation which is approximately an order of magnitude smaller than the minimum strength necessary to detect integrability breaking behavior with r ratios. Our results confirm, at least qualitatively, these findings.

Much more interesting is the behavior for intermediate values of κ, corresponding to the late cluster regime in regime III. In this regime, we find that $\|\tilde{\mathcal{A}}_\lambda(\kappa)\|^2$ scales with N faster than predicted by ETH since curves for different values of N do not collapse on top of each other. This behavior has already been reported in Ref. [29], where it was attributed to a glassylike dynamics and not to a genuine MBL phase. Interestingly, the numerical distinction between regimes II and III was very challenging to observe in Ref. [33]. On the other hand, AGP seems to be very sensitive to this change of regime. We interpret this result as proof that AGP is particularly sensitive to the change of regime of the energy shell, that is, capable of identifying situations where the shell covers just a fraction of the nearest neighbors.

All in all, our results are in excellent agreement with Refs. [29,52], while they only partially agree with the analytical predictions of Ref. [33]. From finite size analysis, it is possible to clearly distinguish just three regimes, instead of the four predicted in the thermodynamic limit: an ergodic regime, a regime with scaling larger than ETH (cluster regime), and finally, the Fock-space localized regime. It is interesting to note that our results indicate, at least qualitatively,

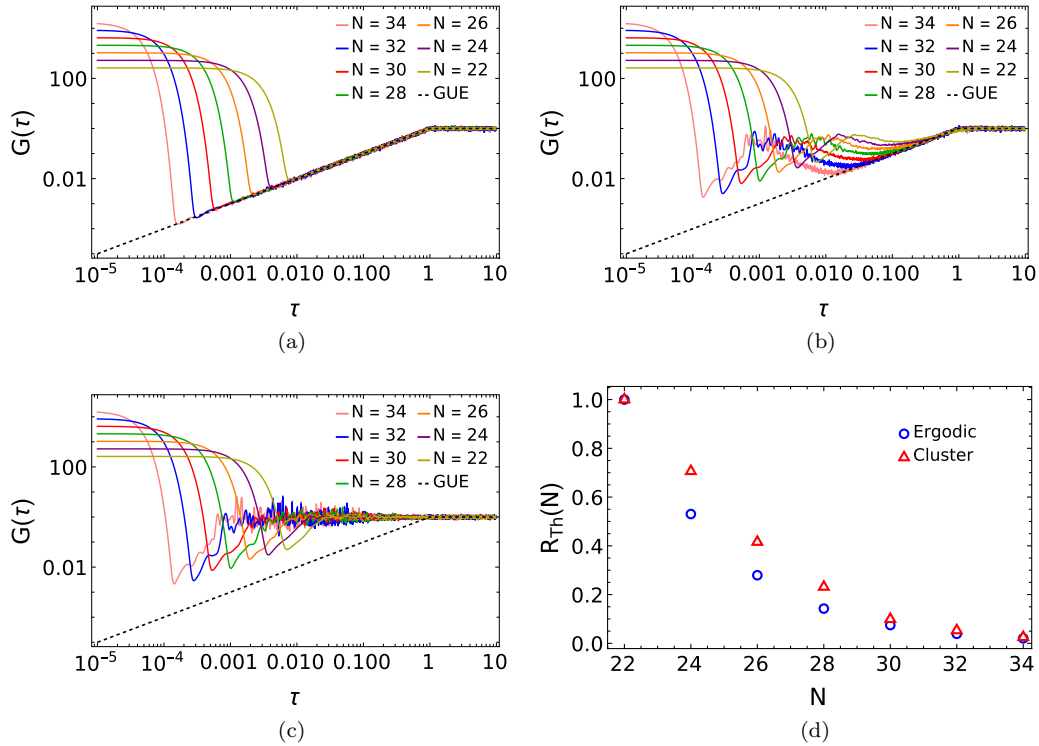

FIG. 2. Spectral form factor in (a) ergodic (I), (b) cluster (III), and (c) Fock-space localized (IV) regimes. While in the ergodic regime, the spectral form factor (SFF) clearly follows the standard random matrix theory (RMT) behavior, in the cluster regime (regime III), the onset of the RMT behavior is considerably delayed. The Fock-space localized regime does not show any RMT behavior. (d) Dependence of $R_{\rm Th}(N)$, Eq. (6), vs system size N.

that they do not depend on the model being all-to-all since they are very similar to those obtained in Refs. [29,52] for local models. While we do not have a complete answer to explain this similarity, we believe it arises because AGP is sensitive to the eigenstates being localized, spread over few nearest neighbors, or ergodically spread in Fock space. The relevant notion of locality is therefore in Fock space, while in real space, it is relevant only to further determine the associated locality in Fock space. Hence, we expect the effects of locality in real space to be rather quantitative than qualitative.

IV. NUMERICAL RESULTS: SPECTRAL FORM FACTOR

Having found that, in the late cluster regime, AGP has a faster scaling with N, we now probe in more detail the thermalizing properties of this regime. Thermalization timescales are often associated with the so-called *Thouless time*, $\tau_{\rm Th}$, which is by definition the time after which quantum evolution becomes universal and described by random matrix theory (RMT), while for shorter times, the behavior is system dependent and nonuniversal, with a bump described and studied in Ref. [53]. Thouless time has been extensively studied recently via the SFF [32,53–56]. Reference [32] investigated some aspects of Thouless time for the mass deformed SYK. However, there, the focus was mainly on the low-temperature region of the SYK spectrum and on the possible hints of scrambling dynamics in the SFF, while an in-depth analysis of the thermalizing properties in regime III was not performed. This is done in this section.

By definition, the SFF is the Fourier transform of the density-density correlation function. For computational purposes, it is more convenient to consider a Gaussian filtered version of it [56]. Concretely, we adopt the definition of Ref. [24]:

$$G(\tau) \equiv \frac{1}{Z}\left\langle \left| \sum_{n=1}^{D} \rho(\epsilon_n) \exp(-i2\pi\epsilon_n\tau) \right|^2 \right\rangle, \tag{5}$$

where Z is a normalizing factor to ensure $G(\tau \gg 1) \approx 1$, the ϵ_n are the unfolded energy levels, and $\rho(\epsilon_n)$ is the Gaussian filtering function; see Appendix D for more details. The time is measured in units of Heisenberg time, which is defined by the inverse of the mean level spacing.

Given these preliminaries, we have computed the SFF for increasing system sizes for three values of κ, i.e., $\kappa = 0.1$, 2.09, and 100. They have been chosen to be well inside the ergodic regime, regime III, and regime IV, respectively [57]. Our results are presented in Figs. 2(a)–2(c). Results for $k = 0.1$ and 100 are in agreement with the expectations: for $k = 0.1$, the SFF shows a robust ramp, in perfect agreement with the RMT prediction and with $\tau_{\rm Th}$ decreasing with increasing system size. Similarly, when $\kappa = 100$, the SFF does not show any agreement with RMT predictions, with $\tau_{\rm Th}$ becoming identical to the Heisenberg time.

Once again, interesting results appear for $\kappa = 2.09$. We see that, at early times, the SFF shows the usual initial decay, followed by an intermediate regime which is not controlled by RMT-like behavior. This early time behavior appears to be

in very good agreement with the analog behavior exhibited by the SFF at large disorder, $\kappa = 100$, for which the full model is essentially controlled by the quadratic SYK_2 Hamiltonian. A faster-than-RMT ramp is clearly visible. For the pure SYK_2 model, the presence of this fast ramp (exponential in time) can be computed analytically in the large-N limit [58–60]. Our analysis shows that the exponential ramp dominates the behavior of the SFF also in a regime of intermediate disorder.

However, at later times, but still earlier than Heisenberg time, the SFF approaches the RMT predictions, showing a ramp in agreement with RMT behavior. The SFF decay—from the exponential ramp to the RMT ramp—looks reminiscent of the transition experienced by the SFF for a bunch of single-particle chaotic models when coupled by nearest neighbor interactions, as described in Ref. [61]. Overall, we see this as a consequence of the interplay between the SYK_2 Hamiltonian and the interacting quartic term, so that $\tau_{\rm Th}$ gets inflated by $\sim$2 orders of magnitude (in units of Heisenberg time).

To better quantify the ergodic properties of the SFF in this regime and to compare them with the analog properties of the SFF in the manifestly ergodic regime, we measured the scaling of Thouless time with N, in units of Thouless time measured at $N = 22$ [62]. In other words, we define the following quantity:

$$R_{\rm Th}(N) \equiv \frac{\tau_{\rm Th}(N)}{\tau_{\rm Th}(22)}, \tag{6}$$

and our results are reported in Fig. 2(d). For small system sizes, the scaling of $R_{\rm Th}$ with N is faster in the ergodic regime. However, the situation starts to change for $N \geqslant 30$, where the scaling in the two regimes becomes comparable. This result strongly supports those of Ref. [29], according to which the regime where AGP scaling is faster than ergodic is a delayed but still thermalizing regime.

V. CONCLUSIONS AND OUTLOOK

We have studied the thermalizing properties of mass-deformed SYK in a regime of intermediate disorder, relying on the analytical results of Ref. [33]. In quantitative terms, this regime—named the cluster regime in this paper—is characterized by eigenstates which are extended but cover only a fraction of the total Hilbert space.

It has been argued in Ref. [16] and further confirmed by several subsequent numerical studies that a proper MBL regime is not a regime in which eigenstates are localized in Fock space—the so-called Fock-space localization discussed in seminal MBL papers [11–13]—but it is a regime in which eigenstates are extended but not ergodically spread over the full Hilbert space. Hence, the cluster regime can be viewed as the all-to-all version of the MBL regime (although in mass deformed SYK, eigenstates are ergodically extended over their support [34]), thus making it particularly suitable for numerical analysis, to be contrasted with the analytical results presented in Ref. [33].

In agreement with Ref. [29], we found that this regime of intermediate disorder has a very clear characterization in terms of the AGP norm, as defined in Eq. (4): it is the regime where the AGP shows scaling with system size which is faster than ETH, dubbed as *maximally chaotic* in Ref. [29].

To better characterize the dynamical features of this regime, we have computed the SFF and have contrasted it with the SFFs computed in the manifestly ergodic and Fock-space localized regimes. The SFF is particularly suitable for such an analysis since it provides an estimate of the timescale, Thouless time $\tau_{\rm Th}$, at which universality arises and can be detected. Our analysis shows that, in this intermediate regime, $\tau_{\rm Th}$ is delayed by $\sim$2 orders of magnitude as compared with $\tau_{\rm Th}$ computed in the manifestly ergodic regime. However, although delayed, it is still clearly smaller than the Heisenberg time. In addition, we have studied the scaling of $\tau_{\rm Th}$ with system size, as compared with the analogous scaling in the manifestly ergodic regime. While at smaller sizes the two scalings are different, these discrepancies become negligible for the largest sizes we could probe, i.e., for $N = 30$, 32, and 34. A previous analysis of the Thouless time scaling for random regular graphs has been performed in Ref. [63], where subdiffusive scaling was identified. Unfortunately, a similar analysis for the late cluster regime is very challenging, given that the only points which could be considered are $N = 30$, 32, and 34. Reaching larger system sizes will be crucial to address this interesting point.

Overall, our results strongly suggest that the late cluster regime should be considered a regime of delayed thermalization, and although such a delay is quantitatively large, so that it could be easily missed in time evolution analysis, the system still appears completely thermalizing. To find a genuinely nonthermalizing regime, i.e., a regime in which Thouless time does coincide with Heisenberg time, one has to go to regime IV, which is the regime of genuine Fock-space localization.

Our results, in agreement with the analysis of Refs. [29,52] (and considering the analytical predictions of Ref. [33]), add to other recent results [36] questioning the usual idea according to which the MBL phase, in disordered models, should not be understood as Fock-space localization and that, in the MBL phase eigenstates, are extended, and the extension scales with system size N. The thermalizing properties of this regime seem to become more prominent with increasing system size. We would also like to point out the possibility that the existence of non-Fock-space-localized MBL might depend on subtle model details, e.g., the type of disorder and interaction, as suggested, for example, in Ref. [64]. On the other hand, we believe that these results clearly show that mass-deformed SYK captures all the interesting features which are at the core of the recent debates on MBL.

Of course, our numerical results, based on full exact diagonalization, are limited to systems of finite size and cannot be taken as definitive results concerning the fate of MBL in the thermodynamic limit. Along this line, it would be extremely important to fully understand

which dynamical mechanism triggers the faster-than-ETH scaling of the AGP. Our results indicate that the formation of an energy shell *per se* is not sufficient. It also needs to become small enough to extend over just a fraction of the neighbors of a given resonant site. Perhaps it could be possible to use the solvability of the mass-deformed SYK to investigate the

behavior of AGP and SFF in the thermodynamic limit in the cluster regime.

Very recently, a toy model has been presented showing a regime with eigenstates being nonergodically extended—unlike the mass-deformed SYK model—and Poissonian statistics [65]. This could be a good avatar to describe genuine models of MBL without Fock-space localization. It will be interesting to characterize this regime through the lens of AGP.

We hope to come back to these points in the near future.

ACKNOWLEDGMENTS

We acknowledge support by the Institute for Basic Science in Korea (No. IBS-R024-D1). We thank Masaki Tezuka for kindly explaining the results of Refs. [33,34]. We thank Boris Altshuler, David J. Luitz, Anatoli Polkovnikov, and Lev Vidmar for interesting discussions and comments.

APPENDIX A: MAPPING TO THE CONVENTIONS OF REF. [33]

To simplify comparison, we map the conventions used in the main text to those of Ref. [33].

To start with, Ref. [33] assumes that the Majorana fermions, here denoted by $\hat{\psi}_i$ (with $i = 1, \ldots, 2M$) to distinguish them from the notation $\hat{\chi}_i$ used in the main text, satisfy the algebra:

$$\{\hat{\psi}_i, \hat{\psi}_j\} = 2\delta_{ij}\,, \tag{A1}$$

implying that $\hat{\chi}_i = \frac{1}{\sqrt{2}}\hat{\psi}_i$ and $2M = N$.

The quartic Hamiltonian of Ref. [33], here denoted by $\hat{\tilde{\mathcal{H}}}_4$, reads

$$\begin{aligned}\hat{\tilde{\mathcal{H}}}_4 &\equiv \frac{1}{4!}\sum_{i,j,k,l=1}^{2M} \tilde{J}_{ijkl}\hat{\psi}_i\hat{\psi}_j\hat{\psi}_k\hat{\psi}_l \\ &= 4\sum_{i<j<k<l=1}^{N} \tilde{J}_{ijkl}\hat{\chi}_i\hat{\chi}_j\hat{\chi}_k\hat{\chi}_l,\end{aligned} \tag{A2}$$

where we made use of the relations in Eq. (A1). The coupling constants $\tilde{J}_{ijkl}$ are Gaussian distributed with mean value zero and variance:

$$\langle \tilde{J}_{ijkl}^2\rangle = \frac{6J^2}{N^3}, \quad J^2 \equiv \frac{2}{M} = \frac{4}{N}, \tag{A3}$$

from which we deduce

$$\tilde{J}_{ijkl} = \frac{2}{\sqrt{N}}J_{ijkl}, \quad \hat{\tilde{\mathcal{H}}}_4 = 4\frac{2}{\sqrt{N}}\hat{\mathcal{H}}_4. \tag{A4}$$

The quadratic part of the Hamiltonian, here denoted by $\hat{\tilde{\mathcal{H}}}_2$, is given by

$$\hat{\tilde{\mathcal{H}}}_2 \equiv \frac{1}{2}\sum_{i,j=1}^{2M} \tilde{J}_{ij}\hat{\psi}_i\hat{\psi}_j = 2\sum_{i<j=1}^{N} \tilde{J}_{ij}\hat{\chi}_i\hat{\chi}_j, \tag{A5}$$

where the couplings $\tilde{J}_{ij}$ are purely imaginary, and they are extracted from a Gaussian distribution having mean value zero and variance equal to

$$\langle |\tilde{J}_{ij}|^2\rangle = \frac{\delta^2}{N}, \tag{A6}$$

with the parameter δ being the mass deformation parameter in Ref. [33].

Denoting by $\hat{\tilde{\mathcal{H}}}$ the total Hamiltonian in Ref. [33], we get

$$\begin{aligned}\hat{\tilde{\mathcal{H}}} &\equiv \hat{\tilde{\mathcal{H}}}_4 + \hat{\tilde{\mathcal{H}}}_2 = 4\frac{2}{\sqrt{N}}\hat{\mathcal{H}}_4 + 2\delta\hat{\mathcal{H}}_2 \\ &= 4\left(\frac{2}{\sqrt{N}}\hat{\mathcal{H}}_4 + \frac{\delta}{2}\hat{\mathcal{H}}_2\right) = 4\hat{\mathcal{H}},\end{aligned} \tag{A7}$$

where $\hat{\mathcal{H}}$ is given in Eq. (1), and we identified the relation $\kappa = \frac{\delta}{2}$ between the mass deformation parameters.

APPENDIX B: AGP FOR A LOCAL OPERATOR

In this Appendix, we compute the AGP, $||\mathcal{A}_\lambda(\kappa)||^2$, as we did in Sec. III, for a completely local operator. In other words, we replace the extensive operator $\hat{O}$, defined in Eq. (3), with the following nonextensive operator:

$$\hat{O}' \equiv i\hat{\chi}_1\hat{\chi}_2. \tag{B1}$$

As already discussed in Sec. III, the behavior of $||\mathcal{A}_\lambda(\kappa)||^2$ does not depend on the choice of Majorana fermions generating $\hat{O}'$, given the all-to-all property of the model under investigation. On the other hand, one may wonder whether the nonextensive property of the operator plays a role. In Fig. 3, we report our results.

The behavior of the plot is qualitatively unchanged when passing from an extensive to a nonextensive operator, with just a few minor quantitative differences. We believe that the reason for this independence on the locality of the operator has to be traced back to the property that, in many-body interacting systems, the relevant notion of locality is in Fock space and not in real space.

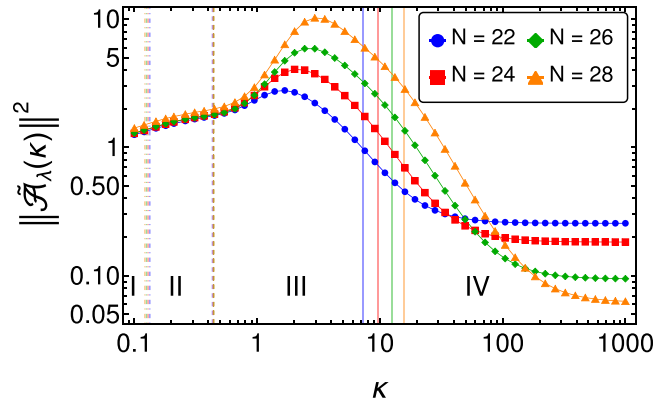

FIG. 3. The behavior of the adiabatic gauge potential (AGP), as a function of the mass deformation strength κ, for the nonextensive operator $\hat{O}'$ defined in Eq. (B1). As we clearly see, the results are barely distinguishable from the analogous results, for an extensive operator, shown in Fig. 1.

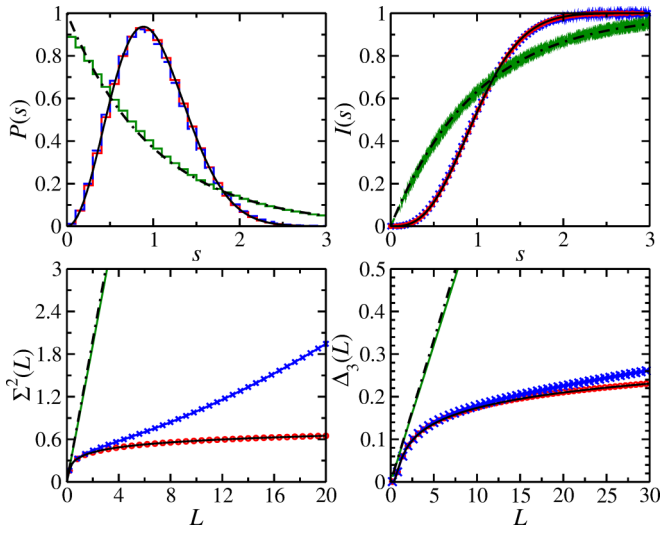

FIG. 4. Comparison of the spectral properties of cases A (red histogram and circles), B (blue histogram and crosses), and C (green histogram and lines), the results for Poissonian random numbers from the GUE (black full lines), and Poissonian random numbers (black dash-dotted lines), respectively.

APPENDIX C: SPECTRAL PROPERTIES

We investigated fluctuation properties in the eigenvalue spectra for the three realizations $\kappa = 0.2, 2.09$, and 100 with $N = 34$ considered in Figs. 2(a), 2(b), and 2(c), referred to as cases A, B, and C in the following. They are compared with RMT results for random matrices from the Gaussian unitary ensemble (GUE). For this, we removed system-specific properties by unfolding the eigenvalues E_j, $E_1 \leqslant E_2 \cdots \leqslant E_D$ independently for each disorder realization to mean spacing unity $\epsilon_j = \bar{N}(E_j)$. The mean integrated spectral density $\bar{N}(E_j)$ is determined by fitting a polynomial of order 12 to the integrated spectral density.

We analyzed short-range correlations in the eigenvalue spectra in terms of the nearest neighbor spacing distribution $P(s)$ of adjacent spacings $s_j = \epsilon_{j+1} - \epsilon_j$ and its cumulant $I(s) = \int_0^s ds' P(s')$, which has the advantage that it does not depend on the binning size of the histograms yielding

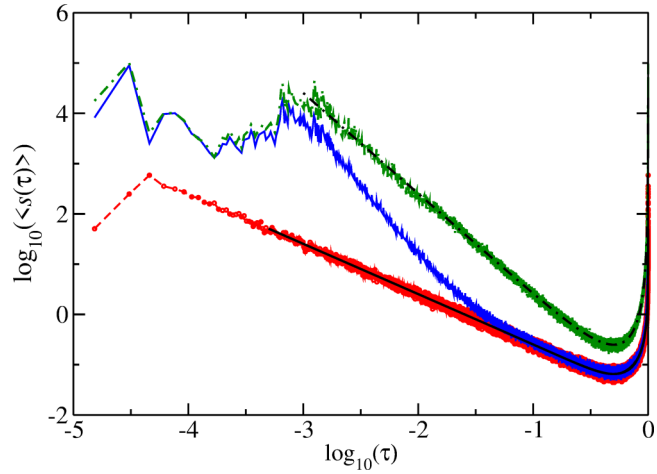

FIG. 5. Same as Fig. 4 for the power spectrum.

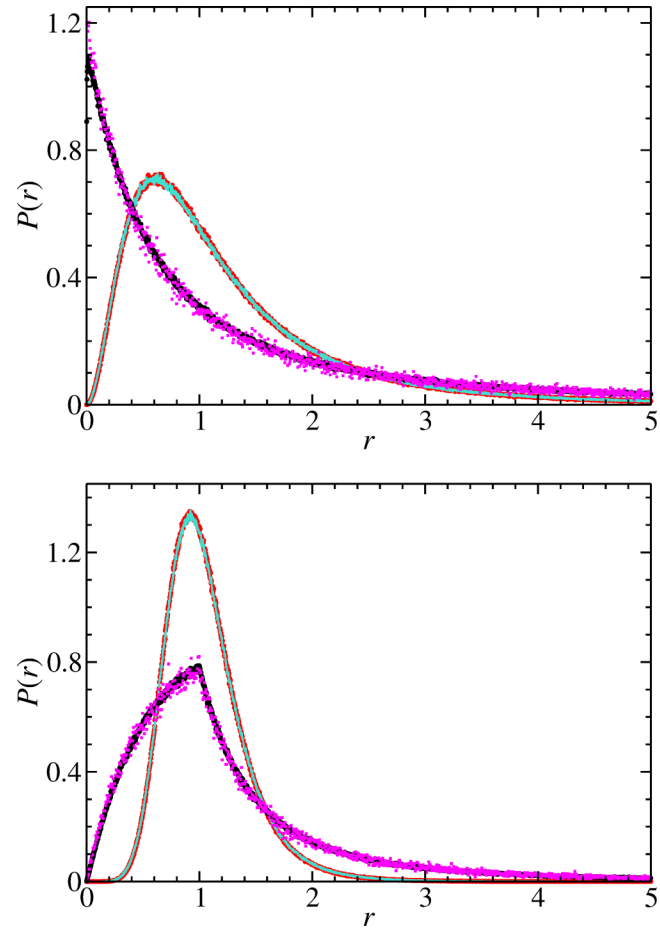

FIG. 6. Comparison of the distributions of the ratios of the spacings between next-nearest $l = 1$ (upper panel) and next-next nearest levels $l = 2$ (lower panel) for the cases A (red dots), B (turquoise line), and C (black dots). For cases A and B, the curves lie on top of each other and on top of the GUE curve; for case C, they lie on top of the curve for 200 000 Poissonian random numbers (magenta squares).

$P(s)$. Another measure for short-range correlations is the distribution of the ratios [18,66] of consecutive spacings between lth nearest neighbors $r_j = \frac{\epsilon_{j+l} - \epsilon_j}{\epsilon_{j+l-1} - \epsilon_{j-1}}$, where we chose $l = 1, \ldots, 10$ and the distribution of $\tilde{r} = \min\{r_j, \frac{1}{r_j}\}$. Ratios are dimensionless, so the nonunfolded eigenvalues can be used [18,66,67]. Furthermore, we considered the variance $\Sigma^2(L) = \langle [N(L) - \langle N(L) \rangle]^2 \rangle$ of the number of unfolded eigenvalues $N(L)$ in an interval of length L, and the rigidity $\Delta_3(L) = \langle \min_{a,b} \int_{e-L/2}^{e+L/2} de [N(e) - a - be]^2 \rangle$ as measures for long-range correlations. Here, $\langle \cdot \rangle$ denotes the average over an ensemble of random matrices or of 100 eigenvalue spectra, each containing 65 536 levels. For the latter, we also performed spectral averages. Furthermore, we analyzed the power spectrum which is given in terms of the Fourier transform of the deviation of the qth nearest neighbor spacing from its mean value q, $\delta_q = \epsilon_{q+1} - \epsilon_1 - q$, from q to τ:

$$s(\tau) = \left\langle \left| \frac{1}{\sqrt{n}} \sum_{q=0}^{n-1} \delta_q \exp(-2\pi i \tau q) \right|^2 \right\rangle, \tag{C1}$$

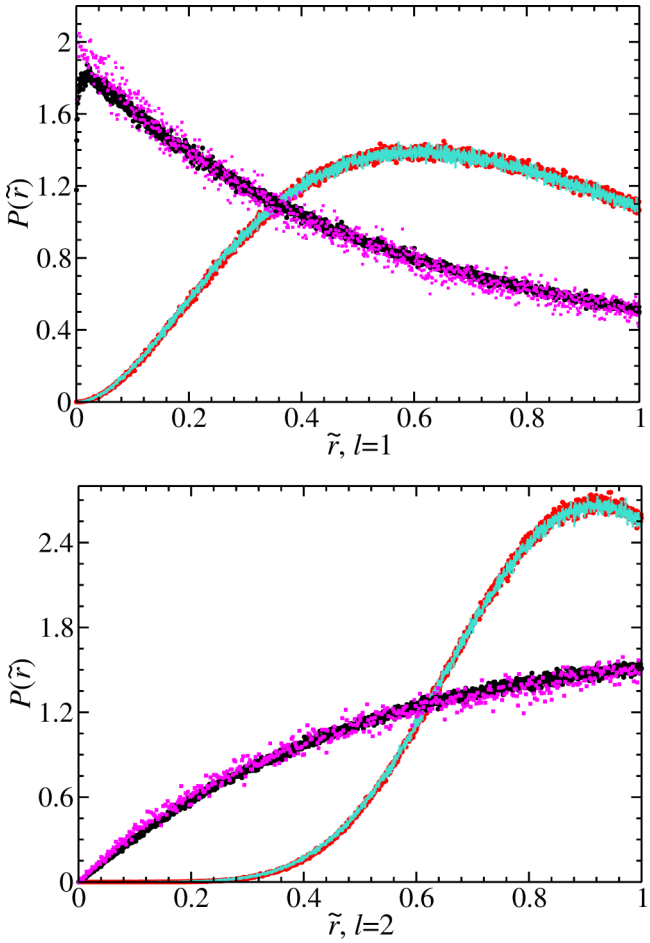

FIG. 7. Same as Fig. 6 for the distributions of $\tilde{r} = \min\{r_j, \frac{1}{r_j}\}$.

for a sequence of n levels, where $0 \leqslant \tau \leqslant 1$. It exhibits for $\tau \ll 1$ a power law dependence $\langle s(\tau)\rangle \propto \tau^{-\alpha}$ [68,69], where for regular systems, $\alpha = 2$, and for chaotic ones, $\alpha = 1$, independently of whether $\mathcal{T}$ invariance is preserved or not [70–75].

In Fig. 4, we compare the spectral properties of the cases A (red histogram and circles), B (blue histogram and crosses), and C (green histogram and lines). They are compared with the RMT prediction for Poissonian random numbers (black dash-dotted lines) and for the GUE (black solid lines). For case A, the curves lie on top of the GUE curves; for case C, they are close to the Poisson curves. The short-range correlations of case B are close to those of case A, whereas we observe clear deviations for the long-range correlations. The same behavior is observed for the power spectra, shown in Fig. 5. The distributions r and $\tilde{r}$, which provide another measure for short-range correlations, are exhibited in Figs. 6 and 7. They agree well with the GUE results for cases A and B and with that of Poissonian random numbers for case C.

For case C, deviations from the results for Poissonian random numbers are only observed for ratios <0.025, whereas the curves for cases B and C lie on top of each other and of the RMT prediction for the GUE. This behavior was also observed for $l = 3, \ldots, 10$. It is in contrast to that observed in the spectral properties, where clear differences are observed.

APPENDIX D: DETAILS ON THE DEFINITION OF SFF

Each ordered energy spectrum $E_1 < E_2 < \cdots < E_D$ is unfolded by fitting the integrated level density with a 12th-order polynomial. The resulting unfolded eigenvalues are denoted by $\epsilon_1 < \epsilon_2 < \cdots < \epsilon_D$. The Gaussian filtering function, $\rho(\epsilon_n)$ is defined as follows:

$$\rho(\epsilon_n) \equiv \exp -\frac{(\epsilon_n - \bar{\epsilon})^2}{2(\eta\Gamma)^2}, \tag{D1}$$

with $\bar{\epsilon}$ and Γ being the mean value and the standard deviation, respectively, of the ensemble realization under consideration. The parameter η determines the effective portion of the spectrum controlling the SFF. It is adjusted to increase the portion of the spectrum considered as much as possible but, at the same time, remove the hard edges of the unfolded spectra.

The prefactor Z is chosen to make the SFF at large time equal to 1, and it is therefore taken equal to $Z \equiv \langle \sum_n |\rho(\epsilon_n)|^2 \rangle$.

[1] J. M. Deutsch, Quantum statistical mechanics in a closed system, Phys. Rev. A **43**, 2046 (1991).

[2] M. Srednicki, Chaos and quantum thermalization, Phys. Rev. E **50**, 888 (1994).

[3] L. D'Alessio, Y. Kafri, A. Polkovnikov, and M. Rigol, From quantum chaos and eigenstate thermalization to statistical mechanics and thermodynamics, Adv. Phys. **65**, 239 (2016).

[4] P. Anderson, Absence of diffusion in certain random lattices, Phys. Rev. **109**, 1492 (1958).

[5] B. Kramer and A. MacKinnon, Localization: theory and experiment, Rep. Prog. Phys. **56**, 1469 (1993).

[6] F. Evers and A. D. Mirlin, Anderson transitions, Rev. Mod. Phys. **80**, 1355 (2008).

[7] D. Hundertmark, A short introduction to Anderson localization, in *Analysis and Stochastics of Growth Processes and Interface Models*, edited by P. Mörters, R. Moser, M. Penrose, H. Schwetlick, and J. Zimmer (Oxford University Press, Oxford, 2008), Chap. 9, p. 194.

[8] D. J. Thouless, A relation between the density of states and range of localization for one dimensional random systems, J. Phys. C **5**, 77 (1972).

[9] P. W. Anderson, D. J. Thouless, E. Abrahams, and D. S. Fisher, New method for a scaling theory of localization, Phys. Rev. B **22**, 3519 (1980).

[10] J. H. Bardarson, F. Pollmann, and J. E. Moore, Unbounded Growth of Entanglement in Models of Many-Body Localization, Phys. Rev. Lett. **109**, 017202 (2012).

[11] B. L. Altshuler, Y. Gefen, A. Kamenev, and L. S. Levitov, Quasiparticle Lifetime in a Finite System: A Nonperturbative Approach, Phys. Rev. Lett. **78**, 2803 (1997).

[12] I. V. Gornyi, A. D. Mirlin, and D. G. Polyakov, Interacting Electrons in Disordered Wires: Anderson Localization and Low-T Transport, Phys. Rev. Lett. **95**, 206603 (2005).

[13] D. Basko, I. Aleiner, and B. Altshuler, Metal–insulator transition in a weakly interacting many-electron system with localized single-particle states, Ann. Phys. **321**, 1126 (2006).

[14] L. Fleishman and P. W. Anderson, Interactions and the Anderson transition, Phys. Rev. B **21**, 2366 (1980).

[15] M. Serbyn, Z. Papić, and D. A. Abanin, Local Conservation Laws and the Structure of the Many-Body Localized States, Phys. Rev. Lett. **111**, 127201 (2013).

[16] B. Bauer and C. Nayak, Area laws in a many-body localized state and its implications for topological order, J. Stat. Mech.: Theory Exp. (2013) P09005.

[17] Marko Žnidarič, T. Prosen, and P. Prelovšek, Many-body localization in the Heisenberg *xxz* magnet in a random field, Phys. Rev. B **77**, 064426 (2008).

[18] V. Oganesyan and D. A. Huse, Localization of interacting fermions at high temperature, Phys. Rev. B **75**, 155111 (2007).

[19] A. Pal and D. A. Huse, Many-body localization phase transition, Phys. Rev. B **82**, 174411 (2010).

[20] V. Ros, M. Müller, and A. Scardicchio, Integrals of motion in the many-body localized phase, Nucl. Phys. B **891**, 420 (2015).

[21] D. A. Huse, R. Nandkishore, and V. Oganesyan, Phenomenology of fully many-body-localized systems, Phys. Rev. B **90**, 174202 (2014).

[22] D. J. Luitz, N. Laflorencie, and F. Alet, Many-body localization edge in the random-field Heisenberg chain, Phys. Rev. B **91**, 081103(R) (2015).

[23] D. J. Luitz, I. M. Khaymovich, and Y. B. Lev, Multifractality and its role in anomalous transport in the disordered XXZ spin-chain, SciPost Phys. Core **2**, 006 (2020).

[24] J. Šuntajs, J. Bonča, T. Prosen, and L. Vidmar, Quantum chaos challenges many-body localization, Phys. Rev. E **102**, 062144 (2020).

[25] J. Šuntajs, J. Bonča, T. Prosen, and L. Vidmar, Ergodicity breaking transition in finite disordered spin chains, Phys. Rev. B **102**, 064207 (2020).

[26] P. Sierant, D. Delande, and J. Zakrzewski, Thouless Time Analysis of Anderson and Many-Body Localization Transitions, Phys. Rev. Lett. **124**, 186601 (2020).

[27] P. Sierant, M. Lewenstein, and J. Zakrzewski, Polynomially Filtered Exact Diagonalization Approach to Many-Body Localization, Phys. Rev. Lett. **125**, 156601 (2020).

[28] D. Abanin, J. Bardarson, G. De Tomasi, S. Gopalakrishnan, V. Khemani, S. Parameswaran, F. Pollmann, A. Potter, M. Serbyn, and R. Vasseur, Distinguishing localization from chaos: Challenges in finite-size systems, Ann. Phys. **427**, 168415 (2021).

[29] D. Sels and A. Polkovnikov, Dynamical obstruction to localization in a disordered spin chain, Phys. Rev. E **104**, 054105 (2021).

[30] A. Morningstar, L. Colmenarez, V. Khemani, D. J. Luitz, and D. A. Huse, Avalanches and many-body resonances in many-body localized systems, Phys. Rev. B **105**, 174205 (2022).

[31] A. M. García-García, B. Loureiro, A. Romero-Bermúdez, and M. Tezuka, Chaotic-Integrable Transition in the Sachdev-Ye-Kitaev Model, Phys. Rev. Lett. **120**, 241603 (2018).

[32] T. Nosaka, D. Rosa, and J. Yoon, The Thouless time for mass-deformed SYK, J. High Energy Phys. 09 (2018) 041.

[33] F. Monteiro, T. Micklitz, M. Tezuka, and A. Altland, Minimal model of many-body localization, Phys. Rev. Res. **3**, 013023 (2021).

[34] F. Monteiro, M. Tezuka, A. Altland, D. A. Huse, and T. Micklitz, Quantum Ergodicity in the Many-Body Localization Problem, Phys. Rev. Lett. **127**, 030601 (2021).

[35] M. Pandey, P. W. Claeys, D. K. Campbell, A. Polkovnikov, and D. Sels, Adiabatic Eigenstate Deformations as a Sensitive Probe for Quantum Chaos, Phys. Rev. X **10**, 041017 (2020).

[36] P. Sierant, E. G. Lazo, M. Dalmonte, A. Scardicchio, and J. Zakrzewski, Constraint-Induced Delocalization, Phys. Rev. Lett. **127**, 126603 (2021).

[37] P. Sierant, M. Lewenstein, and A. Scardicchio, Universality in Anderson localization on random graphs with varying connectivity, arXiv:2205.14614.

[38] P. Sierant, M. Lewenstein, A. Scardicchio, and J. Zakrzewski, Stability of many-body localization in kicked Ising model, arXiv:2203.15697.

[39] J. Kim and X. Cao, Comment on "Chaotic-Integrable Transition in the Sachdev-Ye-Kitaev Model", Phys. Rev. Lett. **126**, 109101 (2021).

[40] A. M. García-García, B. Loureiro, A. Romero-Bermúdez, and M. Tezuka, García-García *et al.* Reply:, Phys. Rev. Lett. **126**, 109102 (2021).

[41] S. Sachdev and J. Ye, Gapless Spin-Fluid Ground State in a Random Quantum Heisenberg Magnet, Phys. Rev. Lett. **70**, 3339 (1993).

[42] J. Maldacena and D. Stanford, Remarks on the Sachdev-Ye-Kitaev model, Phys. Rev. D **94**, 106002 (2016).

[43] J. Polchinski and V. Rosenhaus, The spectrum in the Sachdev-Ye-Kitaev model, J. High Energy Phys. 04 (2016) 001.

[44] We follow the conventions of the seminal paper by Maldacena and Stanford [42]. The details of the mapping from our conventions and results to those of Ref. [33] are reported in Appendix A.

[45] T. Micklitz, F. Monteiro, and A. Altland, Nonergodic Extended States in the Sachdev-Ye-Kitaev Model, Phys. Rev. Lett. **123**, 125701 (2019).

[46] We would like to point out the similarity of such states to the states observed in a 1D model with a maximally correlated disorder [76].

[47] P. Sierant, A. Maksymov, M. Kuś, and J. Zakrzewski, Fidelity susceptibility in Gaussian random ensembles, Phys. Rev. E **99**, 050102(R) (2019).

[48] A. Maksymov, P. Sierant, and J. Zakrzewski, Energy level dynamics across the many-body localization transition, Phys. Rev. B **99**, 224202 (2019).

[49] M. Kolodrubetz, D. Sels, P. Mehta, and A. Polkovnikov, Geometry and non-adiabatic response in quantum and classical systems, Phys. Rep. **697**, 1 (2017).

[50] N. Hunter-Jones, J. Liu, and Y. Zhou, On thermalization in the SYK and supersymmetric SYK models, J. High Energy Phys. 02 (2018) 142.

[51] M. Haque and P. A. McClarty, Eigenstate thermalization scaling in Majorana clusters: from chaotic to integrable Sachdev-Ye-Kitaev models, Phys. Rev. B **100**, 115122 (2019).

[52] T. LeBlond, D. Sels, A. Polkovnikov, and M. Rigol, Universality in the onset of quantum chaos in many-body systems, Phys. Rev. B **104**, L201117 (2021).

[53] V. E. Kravtsov, I. M. Khaymovich, E. Cuevas, and M. Amini, A random matrix model with localization and ergodic transitions, New J. Phys. **17**, 122002 (2015).

[54] J. S. Cotler, G. Gur-Ari, M. Hanada, J. Polchinski, P. Saad, S. H. Shenker, D. Stanford, A. Streicher, and M. Tezuka, Black holes and random matrices, J. High Energy Phys. 05 (2017) 118.

[55] A. M. García-García, Y. Jia, and J. J. M. Verbaarschot, Universality and Thouless energy in the supersymmetric Sachdev-Ye-Kitaev model, Phys. Rev. D **97**, 106003 (2018).

[56] H. Gharibyan, M. Hanada, S. H. Shenker, and M. Tezuka, Onset of random matrix behavior in scrambling systems, J. High Energy Phys. 07 (2018) 124.

[57] Since the SFF is a spectral observable, i.e., it is based on eigenvalues, the relevant separation between regimes III and IV is the one described by analytical predictions (vertical solid lines in Fig. 1).

[58] M. Winer, S.-K. Jian, and B. Swingle, Exponential Ramp in the Quadratic Sachdev-Ye-Kitaev Model, Phys. Rev. Lett. **125**, 250602 (2020).

[59] Y. Liao, A. Vikram, and V. Galitski, Many-Body Level Statistics of Single-Particle Quantum Chaos, Phys. Rev. Lett. **125**, 250601 (2020).

[60] Y. Liao and V. Galitski, Universal dephasing mechanism of many-body quantum chaos, Phys. Rev. Res. **4**, L012037 (2022).

[61] A. Chan, A. De Luca, and J. T. Chalker, Spectral Statistics in Spatially Extended Chaotic Quantum Many-Body Systems, Phys. Rev. Lett. **121**, 060601 (2018).

[62] The case $N = 22$ seems to be smallest value for which a scaling behavior is observed [33].

[63] L. Colmenarez, D. J. Luitz, I. M. Khaymovich, and G. De Tomasi, Subdiffusive Thouless time scaling in the Anderson model on random regular graphs, Phys. Rev. B **105**, 174207 (2022).

[64] P. Sierant and J. Zakrzewski, Challenges to observation of many-body localization, Phys. Rev. B **105**, 224203 (2022).

[65] W. Tang and I. M. Khaymovich, Non-ergodic delocalized phase with poisson level statistics, Quantum **6**, 733 (2022).

[66] Y. Y. Atas, E. Bogomolny, O. Giraud, and G. Roux, Distribution of the Ratio of Consecutive Level Spacings in Random Matrix Ensembles, Phys. Rev. Lett. **110**, 084101 (2013).

[67] Y. Atas, E. Bogomolny, O. Giraud, P. Vivo, and E. Vivo, Joint probability densities of level spacing ratios in random matrices, J. Phys. A: Math. Theor. **46**, 355204 (2013).

[68] A. Relaño, J. M. G. Gómez, R. A. Molina, J. Retamosa, and E. Faleiro, Quantum Chaos and $1/f$ Noise, Phys. Rev. Lett. **89**, 244102 (2002).

[69] E. Faleiro, J. M. G. Gómez, R. A. Molina, L. Muñoz, A. Relaño, and J. Retamosa, Theoretical Derivation of $1/f$ Noise in Quantum Chaos, Phys. Rev. Lett. **93**, 244101 (2004).

[70] J. M. G. Gómez, A. Relaño, J. Retamosa, E. Faleiro, L. Salasnich, M. Vraničar, and M. Robnik, $1/f^{\alpha}$ Noise in Spectral Fluctuations of Quantum Systems, Phys. Rev. Lett. **94**, 084101 (2005).

[71] L. Salasnich, Colored noise in quantum chaos, Phys. Rev. E **71**, 047202 (2005).

[72] M. S. Santhanam and J. N. Bandyopadhyay, Spectral Fluctuations and $1/f$ Noise in the Order-Chaos Transition Regime, Phys. Rev. Lett. **95**, 114101 (2005).

[73] A. Relaño, Chaos-Assisted Tunneling and $1/f^{\alpha}$ Spectral Fluctuations in the Order-Chaos Transition, Phys. Rev. Lett. **100**, 224101 (2008).

[74] E. Faleiro, U. Kuhl, R. Molina, L. Muñoz, A. Relaño, and J. Retamosa, Power spectrum analysis of experimental Sinai quantum billiards, Phys. Lett. A **358**, 251 (2006).

[75] J. Mur-Petit and R. A. Molina, Spectral statistics of molecular resonances in erbium isotopes: How chaotic are they? Phys. Rev. E **92**, 042906 (2015).

[76] A. Duthie, S. Roy, and D. E. Logan, Anomalous multifractality in quantum chains with strongly correlated disorder, Phys. Rev. B **106**, L020201 (2022).